Wireless Electrochemiluminescence Bipolar Electrode Array for Visualized Genotyping of Single Nucleotide Polymorphism

Seyyed Mehdi Khoshfetrat, Mitra Ranjbari, Mohsen Shayan, Masoud A. Mehrgardi, Abolfazl Kiani*

Department of chemistry, University of Isfahan, Isfahan 81746-73441, Iran.

ABSTRACT

The development of simple, inexpensive, hand-held, user-friendly biosensor for High throughput and multiplexed genotyping of various single nucleotide polymorphisms (SNPs) in a single run experiment by a non-specialist user is the main challenge in the analysis of DNA. Visualizing the signal and possibility to monitor SNPs by a digital camera opens a new horizon for the routine applications. In the present manuscript, a novel wireless electrochemiluminescence (ECL) DNA array is introduced for the visualized genotyping of different SNPs on the basis of ECL of luminol/hydrogen peroxide system on a bipolar electrode (BPE) array platform. After modification of anodic poles of the array with the DNA probe and its hybridization with the targets, genotyping of various SNPs is carried out by exposing the array to different monobase modified luminol-platinum nanoparticles (M-L-PtNPs). Upon the hybridization of M-L-PtNPs to mismatch sites, the ECL of luminol is followed using a photomultiplier tube (PMT) or digital camera and the images are analyzed by ImageJ software. This biosensor can detect even thermodynamically stable SNP (G–T mismatches) in the range of 2-600 pM. Also, by combining the advantages of BPE and the high visual sensitivity of ECL, it could be easily expected to achieve sensitive screening of different SNPs. The present biosensor demonstrates the capability for the discrimination between PCR products of normal, hetero- and homozygote Beta thalassemia genetic disorders.

KEYWORDS: Single Nucleotide Polymorphism (SNP); luminol-Platinum Nanoparticles; Bipolar Electrochemistry; Electrochemiluminescence.

A single nucleotide polymorphisms (SNPs) are a single-base variation that can occur in the coding or non-coding regions. SNPs in the coding regions, can lead to diverse responses to drug treatments by altering amino acid sequence and protein structure. SNPs are also susceptible to various common diseases such as hypertension, Alzheimer's disease, cancer and etc.[1]. Therefore, it is extremely crucial to develop a method for the sensitive, simple and rapid detection of SNPs. So far, several technologies have been used for the SNP genotyping such as enzyme/protein-based reaction[2], optical methods[3], gel electrophoresis[4] and electrochemical genosensors[5]. The enzyme/protein-based approaches are limited due to the susceptibility to denaturant under different conditions such as high pH and temperature. Also, not all types of mismatch such as adenine–adenine (A–A), thymine–thymine (T–T) and cytosine–cytosine (C–C) mismatch, can be detected by using these protocols[4, 6]. Optical methods require the modification of probe DNA with fluorophores and quenchers. This in turn makes the procedure complicated and expensive. Gel electrophoresis cannot distinguish between different SNPs at the far end of DNA targets[7]. Electrochemical genosensors offer a promising alternative to carry out applications directed to SNPs[5]. Until now, electrochemical genosensors based on monobase-modified nanoparticles (e.g., nanocrystal quantum dots[8], apoferritin[9], gold nanoparticles[10] and liposomes[11]) have not been extensively studied. In spite of their generally advanced detection strategies and improved detection limits, these methods suffer from some drawbacks, which limit their practical application. These limitations including purification and relatively poor stability of the enzyme, complicated labeling procedures of enzymes or proteins, and harsh condition required for quantum dots based detections lead to complicated and lengthy experimental procedures as well[12]. Also high potential oxidation of AuNPs causes the overlap of signal of gold nanoparticles

(AuNPs) with guanine and adenine that can limit the specificity and selectivity[12b]. Therefore, these protocols are not straightforward for routine and rapid medical analysis.

Recently, our group developed a protocol for simultaneous genotyping of various SNPs based on the electrooxidation of silver nanoparticle (AgNPs) and 1,4 diaminobenzoic acid (DABA)-modified AuNPs[5c]. DABA and also AgNPs can be oxidized at lower potentials and show sharp peaks that causes improvement of the sensitivity and selectivity of the assay. However, that design also suffers from some disadvantages such as double labeling AuNPs which is synthetically demanding, costly and time-consuming. In order to achieve fast and simple protocol, a dual amplification strategy for SNPs detection, using graphene oxide and nanoporous gold electrode, was developed[5b]. In light of demand for sensitive, selective and low-cost with a simple and rapid diagnostics, the integration of bipolar electrochemistry and ECL, would be helpful to circumvent these disadvantages[13]. Among the diverse SNP detection techniques, ECL has become as one of the most versatile methods owing to high sensitivity, wide dynamic response range, good temporal and spatial control and visual imaging capability[14].

In a bipolar electrochemistry (BE), a driving potential is applied through an electrolyte solution containing conducting object (bipolar electrode; BPE) using two feeder electrodes connected to a power supply[15]. This driving potential causes a potential drop in the solution and therefore induces a potential difference along the length of the BPE. If this potential difference is sufficient, the faradaic reactions simultaneously occur at the ends of BPE. A more detailed description of the principles of BE with their applications have been extensively described previously[16]. Recently because of simplicity, low-cost, ease of operation and device fabrication, BE has been applied in a number of interesting analytical studies[17]. Especially this method does

not require a direct electrical connection between BPE and the external power supply (wireless), as a result, using BE allows employing large number of BPE arrays. Recently, integration of BPE and ECL (BPE-ECL), as an important and powerful tool for the molecular recognition platform, have drawn much more attention in bioanalysis[13c, i]. The wireless nature of the BPE and no need for the light source in ECL, not only simplifies detection system for BPE-ECL, but also, improves detection limit and sensitivity, due to no scattered light in the sample and no excitation source fluctuations. Furthermore, there is no limitation on the number of BPEs in an array configuration, and therefore, ECL signals of multiple electrodes can be simultaneously captured using a digital camera[13i, 16b].

The luminol along with hydrogen peroxide (H_2O_2) as its coreactant is a well-known system to produce strong ECL at positive potentials, under a variety of experimental conditions[18]. This ECl system has been applied in the fabrication of the biosensors for the detection of cancer biomarkers[19], thrombin[20], carcinoembryonicantigen[21], IgG[22], the specific anti-hGH antibodies[23] and etc. Recently, the catalytic properties and high loading amount of luminol functionalized nanoparticles for ECL emission, instead of the solution of luminol, have attracted many interest of the researchers. Xu's group reported a novel ECL DNA sensor using luminol-functionalized platinum nanoparticles[24]. Cui et al. developed highly sensitive ECL immunosensorfor detection of Mycobacterium tuberculosis (MTB) using luminol-functionalized gold[25] and silver[26] nanoprobes as labels. Luminol−AuNPs have been also used for the detection of telomerase[27], thrombin[28] and DNA methyltransferase activity[29].

Thalassemia is an inherited blood disorder in which the body makes an abnormal form of hemoglobin, the oxygen-carrying protein inside the red blood cells[30]. Beta thalassemia, with over 200 different β-hemoglobin (HBB) mutations, is one of the thalassemia categories that occur

when a gene or genes related to the Beta globin protein are missing or mutated. Affected people have a shortage of red blood cells (anemia), which can cause pale skin, weakness, fatigue, and more serious complications[31].

In the present research, luminol has been also immobilized on the monobase functionalized nanoparticles. After that, the functionalized nanoparticles accumulated on the electrode surface via hybridization of monobases with mismatch sites.

To the best of our knowledge, up to now, visualized genotyping of SNPs using BPE-ECL array has not been reported. In the present manuscript, a sensitive, selective, simple and rapid BPE-ECL array for SNPs genotyping is investigated. For the BPE array, the signals of each individual anodic poles can be controlled using just two driving electrodes, regardless the number of individual sensing electrodes. To monitor the genotyping of different SNPs, various M-L-PtNPs were employed in the presence of DNA polymerase I (Klenow fragment). In the presence of mismatches, when a sufficiently high electric field is applied across the electrolyte solution, the ECL reaction occurs on the accumulated M-L-PtNPs and H_2O_2 at the anodic poles and this triggers simultaneous O_2 reduction at the cathodic poles. It can be applied for quantitative analysis of SNPs based on capturing of ECL emission upon accumulation of luminol functionalized nanoparticles to mismatch sites using a digital camera. The combination of BE and transduction using a digital camera helps us to develop a very simple and inexpensive method for the SNP genotyping.

Experimental Section

Materials

5-Amino-2, 3-dihydro-1, 4-phthalazinedione (luminol), Tris (hydroxymethyl) aminomethane-Hydrochloride (Tris–HCl), Sodium hydroxide, sodium chloride, potassium chloride, magnesium chloride, sodium hydrogen phosphate, disodium hydrogen phosphate, hydrochloric acid, nitric acid, sulfuric acid, potassium ferrocyanide, potassium ferricyanide, sodium borohydride, sodium citrate trihydrate and Cysteamin hydrochloride were purchased in analytical grade from commercial sources and used as received, without any further purification. Adenosine 5′-triphosphate (ATP), cytidine 5′ triphosphate (CTP), guanosine 5′-triphosphate (GTP), thymidine 5′-triphosphate (TTP) and DNA polymerase I (Klenow fragment), were purchased Vivantis Co. (Malaysia). Nucleobases solutions were prepared using a 20 mM Tris–HCl buffer solution containing 20 mM NaCl (pH 7). Deionized water was used throughout the experiments. The oligonucleotides used in this study were all obtained from Eurofins/MWG/Operon (Germany) and were used as received with following sequences (5' to 3'):

Probe: SH-$(CH_2)_6$- CTG CGT TTT

Complementary (Com): TGC CGA AAA AAA ACG CAG

A-C Mismatch: T**A**C CGA AAA AAA ACG CAG

G-T Mismatch: TGC **T**GA AAA AAA ACG CAG

Capture: TTT TCG GCA.

The stock solution of the oligonucleotides was prepared using PBS 1X (pH 7.4) containing 0.01 M Na_2HPO_4, 0.002 M KH_2PO_4, 0.15 M NaCl and 0.15 M KCl, and kept frozen at -20 ^{OC}. Luminol solutions were prepared using phosphate buffer solution (PBS, pH 7.4) containing 0.1M K_2HPO_4 and 0.1 M KH_2PO_4. The entire modification of electrode surface and hybridizations of probe, target and capture were performed in the 4^{o}C.

Apparatus

Electrochemical impedance spectroscopy (EIS) and cyclic voltammetry (CV) were performed in a three-electrode system containing a small piece of an archival gold compact disc-recordable (gold-CD-R, Memorex, USA) as a working electrode, an Ag/AgCl/3M KCl as a reference electrode and a platinum wire as an auxiliary electrode. EIS experiments were performed at open circuit potential (OCP) by applying an AC potential with a signal amplitude of 5 mV and a frequency range of 10 kHz to 0.1 Hz.

The BE was performed in a home-made electrochemical cell, gold-CD-R as the working electrode[32], and two stainless steel sheets as a driving electrode was used. The bias potential applied between the two stainless steel sheets electrodes was generated by a DC power supply (MASTECH DC Power Supply HY3005F-3) to provide the necessary driving potential. The Surface Plasmon band (SPB) measurements were performed using a JASCOV-670 UV–Vis. spectrophotometer. Scanning electron microscope (SEM) and energy dispersive x-ray spectroscopy (EDX) was carried out with Mira3-TESCAN, at an acceleration voltage of 15 kV. X-ray diffraction (XRD) patterns of the samples were recorded on a Bruker D8/Advance X-ray diffractometer with Cu-K_α radiation at 40 kV and 40 mA.

PCR amplification

For the analysis of the Beta thalassemia genetic disorder in hetero- and homozygote genomic samples, the respective DNAs were separated by using the Viena Lab Kit from blood samples [33]. 100 µL blood sample along with 1mL Lyris solution was incubated 15 minutes in room temperature and centrifuged 3000 rpm for 5 minutes. The resulting supernatant was incubated 5 minutes in 1mL Lyris Solution and centrifuged at 12000 rpm for 10 minutes. The DNA was

subsequently extracted by adding 200µL GenXtract to supernatant; incubated 20 and 10 minutes at 56ºC and 98ºC, respectively.

PCR amplification was performed in a DNA Thermal Cycler ((Mastercycler 5330) using oligonucleotide primers for Beta thalassemia (IVS-II-1).

Forward primer for normal gene (IVS-II-1N):

5'-AAG AAA ACA TCA AGG GTC CCA TAG ACT GAC-3'

Forward primer for mutant gene (IVS-II-1M):

5'-AAG AAA ACA TCA AGG GTC CCA TAG ACT GAT-3'

Reverse primer:

5'-ACCTCACCCTGTGGAGCCAC-3'

The amplification cycle includes: An initial denaturation at 95ºC for 15 min, 35 cycles of amplification consisted of a three-step cycling protocol, 1 min of primer annealing at 95°C, 2 min of extension at 60°C and 90 seconds at 72°C.

Preparation of luminol functionalized Platinum nanoparticles (L-PtNPs)

The L-PtNPs were prepared based on the described procedure in the literature with slight modifications[24]. Briefly a solution containing sodium citrate (5 mL, 38.8 mM) and luminol (1 mL, 10 mM) was added into 10 mL of 1mM $PtCl_6^-$ under heating reflux. After 30 min, the clear solution turned to black. Then the obtained L-PtNPs were cooled down to the room temperature.

Preparation of Monobase-modified L-PtNPs (M-L-PtNPs)

For genotyping of different mismatch types, various monobases including GTP, CTP, ATP or TTP should be attached onto L-PtNPs. For this purpose, L-PtNPs were firstly functionalized by

cysteamine using the addition of 500 μL of 5 mM cysteamin into 500 μL L-PtNPs for 24 h in order to form Pt-S bond. Subsequently, the monobases were covalently bound to the amino group of cysteamine by the formation of a phosphoramidate bond[9a, 10]. Herein, 500 μL of the monobase solution (5 mM) was added to 500 μL of the cysteamine functionalized L-PtNPs and the mixture was shaken for 2 h and centrifuged. The obtained M-L-PtNPs were washed and dispersed in PBS 1X. To genotype various SNPs in a single experimental run and using just one redox ECL probe, nucleobase functionalized L-PtNPs (T-L-PtNPs, C-L-PtNPs, G-L-PtNPs or A-L-PtNPs) were dropped on each individual anodic poles of BPE array.

Fabrication of ECL sensor for the detection of various SNPs:

The procedure details for the fabrication of BPE array has been described in supporting information and Scheme S-1 illustrates a schematic representation of the fabrication steps of a BPE array. Thiolated DNA probe was immobilized on each individual anodic pole of the array according to our previously reported manuscripts[5b, c]. briefly, the probe was deprotected by TCEP and immobilized on the anodic poles through the sulfur-gold chemistry. Subsequently, the modified anodic poles were exposed to various targets along with magnesium chloride to minimize the repulsions between the strands. Finally the capture DNA was hybridized with non-hybridized section of the targets. Herein, to genotype various SNPs, M-L-PtNPs were added to the duplex DNA-coated BPE to hybridize on mismatched sites of the formed duplex DNA strands.

The ECL signals were recorded using a photomultiplier tube (PMT) detector at the set potential of 800 V. In this case, the experiments were performed in a home-made Teflon cell containing two reservoirs with dimensions of 2 × 2 × 1 cm^3 and a channel between these two

reservoirs (length=4 cm, width=0.27 cm). The gold BPE with dimensions of 2.5 × 0.27 cm^2 was placed in the center of the channel of the cell and then the cell was filled with H_2O_2 (2 mM) in PBS buffer (pH 8.5).

In the case of visual imaging, a different cell was designed as the details has been described in supporting information (Scheme S-2). To genotype different SNPs, the ECL signal of the luminol/H_2O_2 was followed as an analytical signal using a Canon EOS 60D digital camera in a dark room with the exposure time of 5 s. The captured ECL images were then analyzed using ImageJ software and the mean color intensity in gray mode for each test zone was determined. Each pixel of a gray scale image has a brightness value ranging from 0 (black) to 255 (white). It should be noted that an individual BPE and a BPE array with the same dimensions, were used for PMT and digital camera transduction, respectively.

Results and Discussion

A BPE is an electrically conductive objective that the electrochemical reactions simultaneously occur at its end of poles in the absence of a direct ohmic contact. The wireless aspect of BPEs makes it possible to apply potential on the array of electrodes using just a single DC power supply or even a battery[16a]. A significant drawback of BE is that the direct current that flows through the BPE is not easy to measure[13i]. This problem can be overcome using the integration of ECL and BPE (BPE-ECL)[34]. Compared to the fluorescence methods, the ECL techniques effectively have no background signal, relatively simple instrumentation and, unlike the fluorescence methods, do not require an external light source[35]. Also, visualization of the signal makes ECL as an attractive method for bioanalysis[14i], since, it can be followed by a simple digital camera or even the naked eye without using any complicated and expensive

instruments[13e]. Moreover, it can be easily implemented in parallel array and thus amenable to simultaneous readout of large array of BPEs.

Preparation and Characterization of L-PtNPs

The L-PtNPs was synthesized based one-pot method by reduction of the platinum salt solution using a solution containing luminol and sodium citrate[24]. The previous reported studies[24-26] demonstrate not only nanoparticles (NPs) exhibit catalytic activity for ECL of luminol molecules, but also causes high loading of luminol on the surface of nanoparticles, that leading to higher sensitivity. The morphology of the resulting L-PtNPs was characterized using scanning electron microscopy (SEM), ultraviolet-visible spectroscopy (UV-Vis), X-ray diffraction (XRD) and energy dispersive x-ray spectroscopy (EDX) as described in supporting information (Figure S-1).

EIS and CV behavior in modification steps

To prove the modification of electrode surface was successfully carried out, the step-by-step modification process has been monitored using EIS and CV techniques. In the EIS Nyquist plots, the semicircle portion at higher frequencies corresponds to the electron transfer resistance (R_{ct}), i.e. semicircle diameter would increase with the increase in R_{ct}. As shows in the Figure S-2A the bare gold electrode (spectrum a) with very small R_{ct}, suggests a fast R_{ct} at the electrode surface. Upon immobilization of the probe on the surface electrode, R_{ct} is increased (spectrum b). Further increase in R_{ct} is observed after the hybridization of the targets with the probe DNA (spectrum c). This is inconsistent with the electrostatic repulsion of the anionic redox indicator negative $Fe(CN)_6^{-3}/Fe(CN)_6^{-4}$ and the phosphate backbone of DNA strands on the surface. Since, the sequence of the complementary and mismatch targets are the same at the lower segments and

complementary to the probe DNA, therefore, no significant differences in the EIS were observed and the spectrum of just complementary target was drawn in the figure. The capture DNA hybridization with the non-hybridized moieties of the targets, also increase the R_{ct} (spectrum d). Subsequently, the modified electrodes were treated using different M-L-PtNPs. It can be seen, when the Com-modified electrode was treated using thymin and guanosine modified L-PtNPs (T/G-L-PtNPs), does not significantly change R_{ct} (spectrum e). This demonstrates that there is no interaction between ds-DNA and M-L-PtNPs and there is no nonspecific adsorption of M-L-PtNs on the electrode surface. On the other hand, when the mismatch targets modified electrodes, A–C (spectrum f) and G–T (spectrum g) mismatches, were subjected to complementary M-L-PtNPs, namely T/G-L-PtNPs and cytosine and adenosine modified L-PtNPs (C/A-L-PtNPs), respectively, R_{ct} obviously decreased, which can be atributed to facilitate electron transfer by PtNPs . The comparison between the R_{ct} of the A–C and G–T mismatches reveals the higher R_{ct} for G-T mismatches, due to the possibility of the formation of hydrogen bonds between guanine and thymine base-pair in the G-T mismatches and less accumulation of PtNPs on the surface. Also, the modification of the electrode surface was followed using CV technique (Figure S-2B). Similar to EIS observations, the immobilization of the probe (voltammogram b) on the surface electrode and subsequently, the hybridization of complementary target (voltammogram c) and then hybridization with the capture (voltammogram d), causes increases in the peak potential separations (ΔE) and decreases in faradic peak currents (I_p), due to the development of negative charges. Also, in agreement with the EIS results, more effective accumulation of PtNPs on A-C mismatch in compared to G-T mismatch, would improve the kinetics and increase I_p and diminish ΔE.

Electrochemiluminescence genotyping of SNPs based BPE-ECL

An ideal SNP assay should be able to discriminate and code all possible SNPs in a simple and an inexpensive manner. The present manuscript describes a fast and cost-effective method to fabricate a high quality, wireless, individually addressable gold electrode array for visualization of different SNPs using a digital camera. The general idea has been illustrated in Scheme 1. As the scheme shows, the mismatch sites were hybridized with their complementary monobases that covalently attached to the nanoparticles. The nanoparticles also modified by luminol and therefore, the ECL intensity of luminol can be followed as an analytical signal. Herein, since the targets are longer than the probe, the hybridization of complementary and mutant targets with self-assembled probe onto the individual anodic poles leads to a structure with a double strand section close to the electrode surface and a non-hybridized single strand section far from the surface of the electrode. After capture hybridization with non-hybridized moiety of the resulting DNA, the modified electrodes are then exposed to different M-L-PtNPs to hybridize base complementary to the mutation sites in the presence of DNA polymerase (Klenow fragment). To remove non-specifically adsorbed nanoparticles on the surface, it was extensively washed by the buffer solution. The EDX spectrum of this modified surface confirms the presence of L-PtNPs on the electrode surface (Figure S-3).

Scheme 1.

For preliminary studies, measurements of the ECL intensities were performed using a PMT as a detector. While PMT offers very good internal amplification gain and so it is one of the most

sensitive transduction systems, it cannot be used for the simultaneous measurements of ECL intensities on each individual arrays. Therefore, for the simultaneous analysis of several samples in a single experiment run, the measurements of ECL intensities through each individual electrode in the array were performed by capturing a digital image and its analysis. It can lead to high throughput multiplexed detection and lower cost per analysis.

ECL-BPE SNP genotyping using PMT detector

To optimize E_{tot}, the ECL intensity-E_{tot} plot of A-C modified BPE, in the presence of the T/G-L-PtNPs was recorded (Figure S-4). The ECL intensities sharply increase with the increase of E_{tot} over the range of 0 to 4.5 V which can be attributed to the ECL reaction of luminol/H_2O_2 at the anodic pole of BPE. The ECL intensities subsequently decrease by more increase in E_{tot} and when E_{tot} exceeds 7.5 V, the ECL emission turns approximately off. At the high overpotential, background reactions, such as the oxidation of water and H_2O_2 initiate and this in turn leads to the formation of oxygen bubbles that could interfere with ECL of lumionl.

The ECL intensities of DNA-modified BPEs in different modification steps were also investigated. As Figure S-5 reveals, no ECL emissions are observed on the bare electrode surface (curve a), Probe DNA (curve b), targets (curve c) and capture modified electrodes (curve d). However, the strong ECL signal is observed after the treatment of A-C mismatch target with T/G-L-PtNPs (curve e). Also, a weaker emission signal can be observed when the G-T mismatch-modified electrode is treated with C/A-L-PtNPs (curve f), due to its more thermodynamically stability. The treatment of the Com target with T/G-L-PtNPs shows no ECL emission (curve g). Thus, the successful analysis of mutants is attributed to the coupling of L-PtNPs to the mutant assembly and labeling of luminol molecules on PtNPs.

To genotype different SNPs using a PMT detector, the ECL emissions of each individual target-modified electrodes were monitored in the presence of various M-L-PtNPs at E_{tot}=4.5 V in several experiment runs. Four A-C modified BPEs were separately subjected to A-L-PtNPs (a), T-L-PtNPs (b), C-L-PtNPs (c) and G-L-PtNPs (d). As Figure 1 reveals, the intermittent ECL signals off and on demonstrate that the sensor shows an excellent sensing selectivity and is feasible for the different genotyping of another mismatch types. For genotyping of G-T mismatches, similar procedure was also carried out in the presence of G-L-PtNPs (e), C-L-PtNPs (f), T-L-PtNPs (g) and A-L-PtNPs (h), respectively. As we expect from hybridization events, the ECL emission from the C-L-PtNPs and A-L-PtNPs, implying the presence of G-T mismatch in the target.

Figure 1.

The quantitative behavior of the ECL biosensor was assessed in response to various concentrations of thermodynamicaly stable G-T mismatch target. Figure 2 shows the ECL intensities versus different G-T mismatch concentrations. The ECL peak intensities increase linearly with the G-T mismatch concentrations over the range of 10-800 pM.

Figure 2.

The stability of PBE-ECL genosensor was also followed by performing eight experiments on a single BPE. As Figure S-6 shows, an acceptable variations on the signals with the RSD less than 5% is observed, which signified that the ECL biosensor reveals good stability.

The main goal of this study is simultaneous to visualize genotyping of various mismatches. For this purpose, the modified anodic poles of a BPE array with various targets were exposed to different M-L-PtNPs. Figure 3A shows an optical graph of array that consists of nine BPEs. As shown in this Figure, each individual electrodes of the array were numbered from 1 to 9. The emitted lights of luminol/H_2O_2 on the anodic poles of the BPEs are captured by the digital camera. Figure 3B and 3C show the image of the array and the ECL intensity Plot of the same region shown in Figure 3A, respectively. The electrodes 1 to 4 were modified with A-C mismatches and each electrode was treated by different M-L-PtNPs, i.e. A-L-PtNPs (1), T-L-PtNPs (2), C-L-PtNPs (3) and G-L-PtNPs (4) (Scheme 1). Since the adenosine and cytosine bases in the A-C mismatch site are complementary with thymine and guanine, the hybridization would be taken place when the modified electrodes were treated with T-L-PtNPs (2) and G-L-PtNPs (4). Therefore, as the figure shows, the blue lights are just observed for (2) and (4) and no lights for (1) and (3) are observed. Also, to prove the prepared biosensor is capable to discriminate between different mismatches, genotyping of G-T mismatch target was carried out (electrodes 5-8, Scheme 1). The ECL image was captured after sequential treatment of 5 to 8 electrodes again with G-L-PtNPs, C-L-PtNPs, T-L-PtNPs and A-L-PtNPs, respectively. In G-T mismatch site, G and T bases are complementary with of C and A on the C-L-PtNPs and A-L-PtNPs, respectively, and it leads to the observation of the blue light on (6) and (8) and no light again on (5) and (7). As mentioned above, the hybridization of the complementary monobases on the L-PtNPs with mismatch sites causes the accumulation of these modified nanoparticles on the surface and the emission of a blue light.

Moreover, the control experiment was carried out using complementary DNA target on the electrode number (9) and treated with T/G-L-PtNPs. Since, the complementary target forms a perfect double strand on the electrode surface, the monobases of M-L-PtNPs would not be hybridized with them and so no light is observed. It suggests the non-specific adsorptions of M-L-PtNPs are not significant and the hybridization takes place just through the specific base pairing as well. This strategy enables us to genotype different SNPs in a very simple, fast fashion with no need to complicated detection instrumental.

Figure 3.

To further demonstrate that the observed emission is directly originated by binding of PtNPs and no by non-uniformity of an electric field or ΔE_{elec}, ECL intensities of luminol (4 μM) in the solution on the bare BPE array were monitored. When a voltage of E_{tot} =5.5 V is applied to the driving electrodes a uniform ECL signal is observed on each individual anodic pole of the array (Figure 4A). The plot of ECL intensities of each individual poles are reasonably uniform (Figure 4B), with relative standard deviation less than 10%, that indicating the ΔE_{elec} and electric field are uniform over the entire array.

Figure 4.

Figure 5 depicts the ECL behavior of the luminol/H_2O_2 system for the different concentrations of the G-T mismatch target. Apparently, when the concentration of G-T mismatch targets increase, the ECL intensities are obviously enhanced. By increasing the concentration of G-T mismatch target, accumulation of PtNPs on the modified anodic poles are increased and cause

enhancement of ECL intensity. A linear log–log relationship between the ECL image gray value and G-T mismatch target concentration is obtained in the concentration range of 2-600 pM.

Figure 5.

Figure S-7 shows the agarose (2.5 %) gel electrophoresis of PCR products. The lanes 1, 3 and 5 show the PCR products of normal, heterozygote and homozygote PCR products, respectively that amplified using IVS-II-1N. The lanes 2, 4 and 6 depict the PCR products of normal, heterozygote and homozygote PCR products, respectively that amplified using IVS-II-1M. IVS-II-1N and IVS-II-1M primers are fully complementary with normal and mismatched genes respectively. The single-base mismatch is at the distal end, therefore, the PCR is done in the case of IVS-II-1N primer with normal genes. Similarly, in the presence of heterozygote genes, the PCR will be done for both IVS-II-1N and IVS-II-1M primers. Finally in the case of homozygote genes the PCR is fulfilled about IVS-II-1M primers[33].

In order to the analysis of PCR products of real samples, an electrode array with 6 individual electrodes was constructed (Figure 6). For the immobilization of PCR product on the gold electrode, 10 μL of cysteamine (20 mM) was self-assembled on the individual cleaned gold electrodes of the array for 8h at room temperature. The resulting modified electrode was thoroughly rinsed with water to remove physically adsorbed cysteamine. Subsequently, 10 μL IVS-II-1N was dropped onto the cysteamine modified electrodes to form a phosphoramidate bond between amino group of cysteamine and free phosphate groups of 5' primers[36]. Then 10 μL of 100-fold diluted PCR products with BPS 1X, were casted on the electrode surface for hybridization of DNAs with immobilized primers on the surface. For this purpose, on the electrode numbers of 1 to 6, the PCR products of lanes 1 to 6agaros gel. It should be noted,

before the casting of PCR products on the electrodes, they were denatured by incubation at 90°C for 15 min followed by rapid cooling in an ice bath. The resulting electrodes were reacted with the G-L-PtNPs, followed by the capture ECL image, as described above. As we expected, the ECL is observed for the PCR products of normal gene has been done with IVS-II-1N (electrode 1), while no light is observed for the PCR products of normal gene has been done with IVS-II-1M (electrode 2). For the heterozygote samples the light is observed for both PCR products that have been done with IVS-II-1N and IVS-II-1M. Finally, since homozygote samples are include only mismatched genomic samples, the light is observed only for the sample that has been amplified with IVS-II-1M (electrode 6).

Figure 6.

Conclusion

In summary, a novel wireless ECL strategy is reported for the visualizing different SNPs on the basis of gold BPE array (BPE-ECL). Due to the catalytic ability of the PtNPs and high loading amount of luminol on the nanoparticles, the ECL intensities are enhanced dramatically and therefore it leads to an ultrahigh sensitive protocol for genotyping of different mismatches upon the hybridization of complementary of M-L-PtNPs to mismatch sites. , There is a linear log - log relationship between the concentration of G-T mismatch targets and image gray value in the linear range of 2-600 pM. This biosensor shows a simple, rapid and efficient strategy for visualized genotyping of different mismatches. This protocol does not need to complicated instruments. Since large number of arrays can be run with a battery as a power supply, and easily integrated with a digital camera, it is promising to develop ECL high throughput screening systems for the genotyping of all different SNPs. Also, the capability of the system for the

analysis of beta thalassemia samples opens new horizons for the application of this method for sensitive diagnosis of genetic disease.

ACKNOWLEDGMENT

We gratefully acknowledge the support of this work by the Research Council of University of Isfahan. Also, the authors would like to express their deepest gratitude to Prof. Sadegh Valian-Boroujeni for generous providing of PCR samples.

AUTHOR INFORMATION

Corresponding Author

*Corresponding author.Tel.: +98 3117932710;fax: +98 3116689732.

E-mail addresses: m.mehrgardi@chem.ui.ac.ir, m.mehrgardi@gmail.com (M.A. Mehrgardi)

REFERENCES

1. (a) R. Sachidanandam, D. Weissman, S. C. Schmidt, J. M. Kakol, L. D. Stein, G. Marth, S. Sherry, J. C. Mullikin, B. J. Mortimore, D. L. Willey, *Nature* **2001,** *409*. 928-933; (b) K. Chen, M. D. McLellan, L. Ding, M. C. Wendl, Y. Kasai, R. K. Wilson, E. R. Mardis, *Genome res.* **2007,** *17*. 659-666; (c) S. Kim, A. Misra, *Annu. Rev. Biomed. Eng.* **2007,** *9*. 289-320.

2. (a) F. Patolsky, A. Lichtenstein, I. Willner, *Nat. Biotechnol.* **2001,** *19*. 253-257; (b) I. K. Litos, P. C. Ioannou, T. K. Christopoulos, J. Traeger-Synodinos, E. Kanavakis, *Anal. Chem.* **2007,** *79*. 395-402; (c) P. Hardenbol, F. Yu, J. Belmont, J. MacKenzie, C. Bruckner, T. Brundage, A. Boudreau, S. Chow, J. Eberle, A. Erbilgin, *Genome res.* **2005,** *15*. 269-275.

3. T. N. Grossmann, L. Röglin, O. Seitz, *Angew. Chem. Int. Ed.* **2007,** *46*. 5223-5225.

4. I. V. Kourkine, C. N. Hestekin, B. A. Buchholz, A. E. Barron, *Anal. Chem.* **2002,** *74*. 2565-2572.

5. (a) G. Liu, T. M. Lee, J. Wang, *J. Am. Chem. Soc.* **2005,** *127*. 38-39; (b) S. M. Khoshfetrat, M. A. Mehrgardi, *Analyst* **2014**; (c) S. M. Khoshfetrat, M. A. Mehrgardi, *ChemElectroChem* **2014,** *1*. 779-786; (d) A. A. Gorodetsky, A. Ebrahim, J. K. Barton, *J. Am. Chem. Soc.* **2008,** *130*. 2924-2925.

6. R. Youil, B. W. Kemper, R. Cotton, *Proc. Natl. Acad. Sci.* **1995,** *92*. 87-91.

7. K. Kerman, D. Ozkan, P. Kara, B. Meric, J. J. Gooding, M. Ozsoz, *Anal. Chim. Acta.* **2002,** *462*. 39-47.

8. (a) G. Liu, T. M. H. Lee, J. Wang, *J. Am. Chem. Soc.* **2005,** *127*. 38-39; (b) M. Ye, Y. Zhang, H. Li, Y. Zhang, P. Tan, H. Tang, S. Yao, *Biosens. Bioelectron.* **2009,** *24*. 2339-2345.

9. (a) G. Liu, Y. Lin, *J. Am. Chem. Soc.* **2007,** *129*. 10394-10401; (b) A. Abbaspour, A. Noori, *Biosens. Bioelectron.* **2012,** *37*. 11-18.

10. K. Kerman, M. Saito, Y. Morita, Y. Takamura, M. Ozsoz, E. Tamiya, *Anal. Chem.* **2004,** *76*. 1877-1884.

11. I. Willner, F. Patolsky, Y. Weizmann, B. Willner, *Talanta* **2002,** *56*. 847-856.

12. (a) M. Holzinger, A. Le Goff, S. Cosnier, *Name: Front. Chem.* **2014,** *2*. 63; (b) D. Lin, J. Wu, M. Wang, F. Yan, H. Ju, *Anal. Chem.* **2012,** *84*. 3662-3668.

13. (a) M.-S. Wu, B.-Y. Xu, H.-W. Shi, J.-J. Xu, H.-Y. Chen, *Lab on a Chip* **2011,** *11*. 2720-2724; (b) M.-S. Wu, G.-s. Qian, J.-J. Xu, H.-Y. Chen, *Anal. Chem.* **2012,** *84*. 5407-5414; (c) K.-F. Chow, F. Mavré, J. A. Crooks, B.-Y. Chang, R. M. Crooks, *J. Am. Chem. Soc.* **2009,** *131*. 8364-8365; (d) T. Wang, S. Fan, R. Erdmann, C. Shannon, *Langmuir* **2013,** *29*. 16040-16044; (e) M.-S. Wu, D.-J. Yuan, J.-J. Xu, H.-Y. Chen, *Chem. Sci.* **2013,** *4*. 1182-1188; (f) M.-S. Wu, D.-J. Yuan, J.-J. Xu, H.-Y. Chen, *Anal. Chem.* **2013,** *85*. 11960-11965; (g) X. Zhang, C. Chen, J. Li, L. Zhang, E. Wang, *Anal. Chem.* **2013,** *85*. 5335-5339; (h) H.-W. Shi, M.-S. Wu, Y. Du, J.-J. Xu, H.-Y. Chen, *Biosens. Bioelectron.* **2014,** *55*. 459-463; (i) K.-F. Chow, F. Mavré, R. M. Crooks, *J. Am. Chem. Soc.* **2008,** *130*. 7544-7545.

14. (a) S. Wu, Z. Zhou, L. Xu, B. Su, Q. Fang, *Biosens. Bioelectron.* **2014,** *53*. 148-153; (b) Y.-L. Chang, R. E. Palacios, F.-R. F. Fan, A. J. Bard, P. F. Barbara, *J. Am. Chem. Soc.* **2008,** *130*. 8906-8907; (c) L. Xu, Y. Li, Y. He, B. Su, *Analyst* **2013,** *138*. 2357-2362; (d) L. Xu, Y. Li, S. Wu, X. Liu, B. Su, *Angewandte Chemie* **2012,** *124*. 8192-8196; (e) N. P. Sardesai, J. C. Barron, J. F. Rusling, *Anal. Chem.* **2011,** *83*. 6698-6703; (f) F. Deiss, C. N. LaFratta, M. Symer, T. M. Blicharz, N. Sojic, D. R. Walt, *J. Am. Chem. Soc.* **2009,** *131*. 6088-6089; (g) D. P. Wasalathanthri, V. Mani, C. K. Tang, J. F. Rusling, *Anal. Chem.* **2011,** *83*. 9499-9506; (h) D. P. Wasalathanthri, S. Malla, I. Bist, C. K. Tang, R. C. Faria, J. F. Rusling, *Lab on a chip* **2013,** *13*. 4554-4562; (i) S. Deng, H. Ju, *Analyst* **2013,** *138*. 43-61.

15. (a) F. o. Mavré, R. K. Anand, D. R. Laws, K.-F. Chow, B.-Y. Chang, J. A. Crooks, R. M. Crooks, *Anal. Chem.* **2010,** *82*. 8766-8774; (b) N. Dorri, P. Shahbazi, A. Kiani, *Langmuir* **2014,** *30*. 1376-1382.

16. (a) F. Mavré, K.-F. Chow, E. Sheridan, B.-Y. Chang, J. A. Crooks, R. M. Crooks, *Anal. Chem.* **2009,** *81*. 6218-6225; (b) S. E. Fosdick, K. N. Knust, K. Scida, R. M. Crooks, *Angew. Chem. Int. Ed.* **2013,** *52*. 10438-10456.

17. (a) E. Sheridan, K. N. Knust, R. M. Crooks, *Analyst* **2011,** *136*. 4134-4137; (b) K.-F. Chow, B.-Y. Chang, B. A. Zaccheo, F. Mavré, R. M. Crooks, *J. Am. Chem. Soc.* **2010,** *132*. 9228-9229.

18. (a) Y.-P. Dong, H. Cui, C.-M. Wang, *J. Phys. Chem. B* **2006,** *110*. 18408-18414; (b) H. Cui, W. Wang, C. F. Duan, Y. P. Dong, J. Z. Guo, *Chem. Eur. J.* **2007,** *13*. 6975-6984; (c) X. Liu, W. Niu, H. Li, S. Han, L. Hu, G. Xu, *Electrochem. Commun.* **2008,** *10*. 1250-1253.

19. (a) S. Xu, Y. Liu, T. Wang, J. Li, *Anal. Chem.* **2011,** *83*. 3817-3823; (b) X. Jiang, H. Wang, R. Yuan, Y. Chai, *Biosens. Bioelectron.* **2015,** *63*. 33-38.

20. Y.-P. Dong, T.-T. Gao, Y. Zhou, J.-J. Zhu, *Anal. Chem.* **2014,** *86*. 11373-11379.

21. X. Jiang, Y. Chai, H. Wang, R. Yuan, *Biosens. Bioelectron.* **2014,** *54*. 20-26.

22. L. Xiao, Y. Chai, R. Yuan, Y. Cao, H. Wang, L. Bai, *Talanta* **2013,** *115*. 577-582.

23. A. Ramanaviciene, N. German, A. Kausaite-Minkstimiene, J. Voronovic, J. Kirlyte, A. Ramanavicius, *Biosens. Bioelectron.* **2012,** *36*. 48-55.

24. H.-R. Zhang, J.-J. Xu, H.-Y. Chen, *Anal. Chem.* **2013,** *85*. 5321-5325.

25. Y. Chai, D. Tian, W. Wang, H. Cui, *Chem. Commun.* **2010,** *46*. 7560-7562.

26. Y. He, D. Liu, X. He, H. Cui, *Chem. Commun.* **2011,** *47*. 10692-10694.

27. H.-R. Zhang, M.-S. Wu, J.-J. Xu, H.-Y. Chen, *Anal. Chem.* **2014,** *86*. 3834-3840.

28. F. Li, H. Cui, *Biosens. Bioelectron.* **2013,** *39*. 261-267.

29. H.-F. Zhao, R.-P. Liang, J.-W. Wang, J.-D. Qiu, *Biosens. Bioelectron.* **2015,** *63*. 458-464.

30. J. Old, *Blood Reviews* **2003,** *17*. 43-53.

31. M. Karimi, N. Cohan, V. De Sanctis, N. S. Mallat, A. Taher, *J. Pediatr. Hematol. Oncol.* **2014,** *31*. 583-596.

32. A. Kiani, E. N. Fard, *Electrochim. Acta* **2009,** *54*. 7254-7259.

33. Z. Rahimi, A. Muniz, A. Parsian, *Mol. Biol. Rep.* **2010,** *37*. 149-154.

34. A. Arora, J. C. Eijkel, W. E. Morf, A. Manz, *Anal. Chem.* **2001,** *73*. 3282-3288.

35. M. M. Richter, *Chem. Rev.* **2004,** *104*. 3003-3036.

36. D. L. Woodyear, T. Campbell, CN Heller, *J. Am. Chem. Soc.* **1996,** *118*. 5504-5505.

Figure Captions:

Scheme 1. Modification of anodic poles of BPE array with DNA targets in the presence of different M-L-PtNPs.

Figure 1. A-C modified BPEs subjected to A-L-PtNPs (a), T-L-PtNPs (b), C-L-PtNPs (c) and G-L-PtNPs (d). G-T modified BPEs in the presence of G-L-PtNPs (e), C-L-PtNPs (f), T-L-PtNPs (g) and A-L-PtNPs (h).

Figure 2. The ECL intensities for the various concentrations of thermodynamicaly stable G-T mismatch target using PMT detector (A) and its Calibration curve (B).

Figure 3. (A) Optical graph of BPE array, (B) The ECL emitted on the anodic poles of BPE array in the presence of various M-L-PtNPs for SNPs genotyping, (C) The ECL image gray value vs. electrode numbers.

Figure 4. (A) The ECL intensities emitted at E_{tot} 5.5 V form bare gold BPE array, (B) The ECL intensity histogram for the bare gold BPE array.

Figure 5. (A) The ECL image of the anodic poles at different concentrations of G-T mismatch, (B) Calibration curve of ECL image gray value for the concentration of G-T mismatch target.

Figure 6. The ECL image of the anodic poles for PCR products of real sample. Electrode 1: PCR product of normal genes amplified in presence of IVS-II-1N; Electrode 2: PCR product of normal genes amplified in presence of IVS-II-1M; Electrode 3: PCR product of heterozigote genes amplified in presence of IVS-II-1N; Electrode 4: PCR product of heterozigote genes amplified in presence of IVS-II-1M; Electrode 5: PCR product of homozigote genes amplified in

presence of IVS-II-1N; Electrode 6: PCR product of homozigote genes amplified in presence of IVS-II-1M;

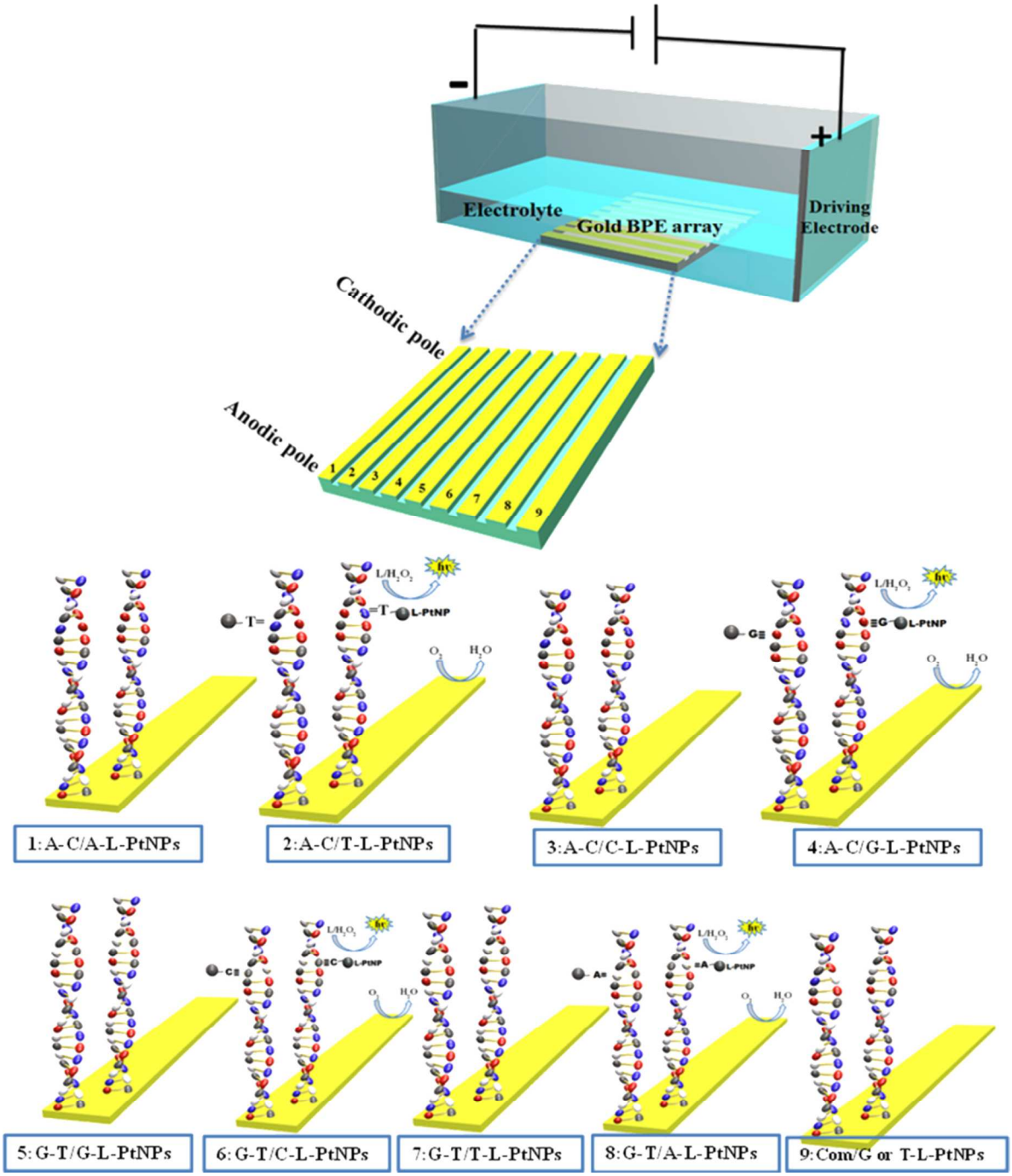
Electrolyte
Gold BPE array
Driving Electrode
Cathodic pole
Anodic pole
1
2
3
4
5
6
7
8
9
1:A-C/A-L-PtNPs
2:A-C/T-L-PtNPs
3:A-C/C-L-PtNPs
4:A-C/G-L-PtNPs
5:G-T/G-L-PtNPs
6:G-T/C-L-PtNPs
7:G-T/T-L-PtNPs
8:G-T/A-L-PtNPs
9:Com/G or T-L-PtNPs

Scheme 1.

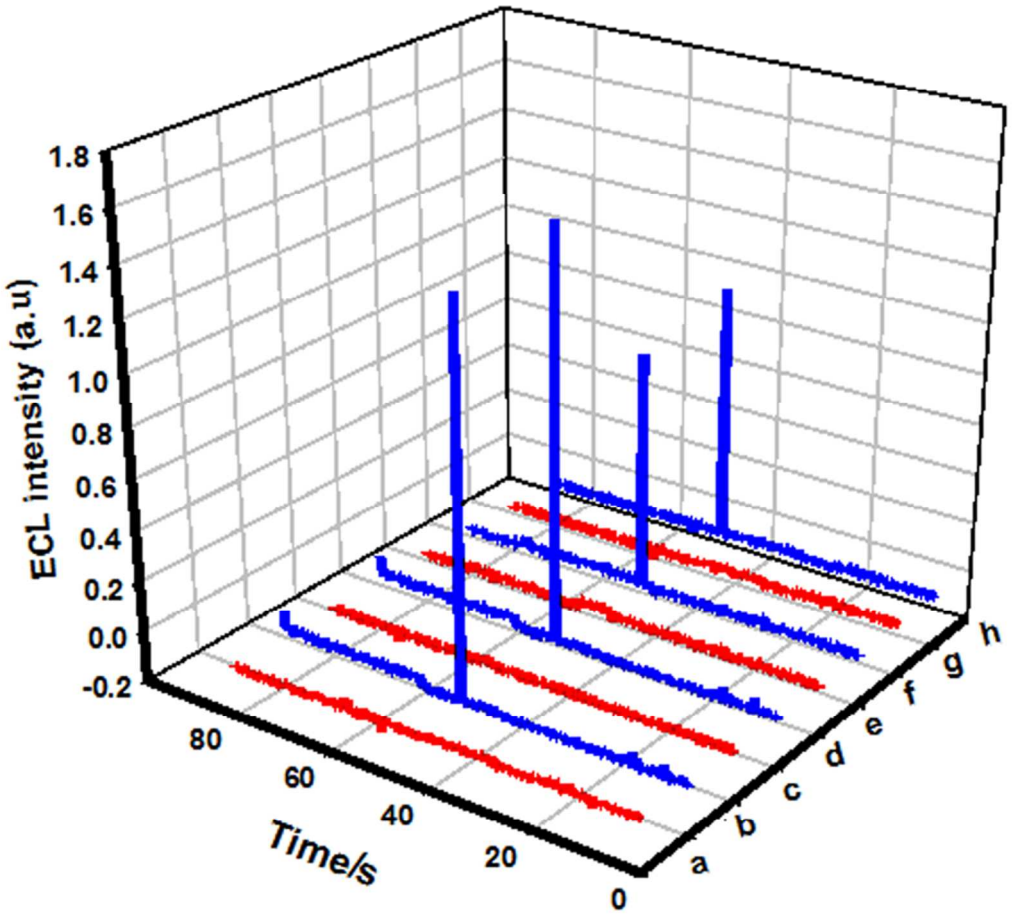
ECL intensity (a.u)
1.8
1.6
1.4
1.2
1.0
0.8
0.6
0.4
0.2
0.0
-0.2
80
60
40
20
0
Time/s
a
b
c
d
e
f
g
h

Figure 1.

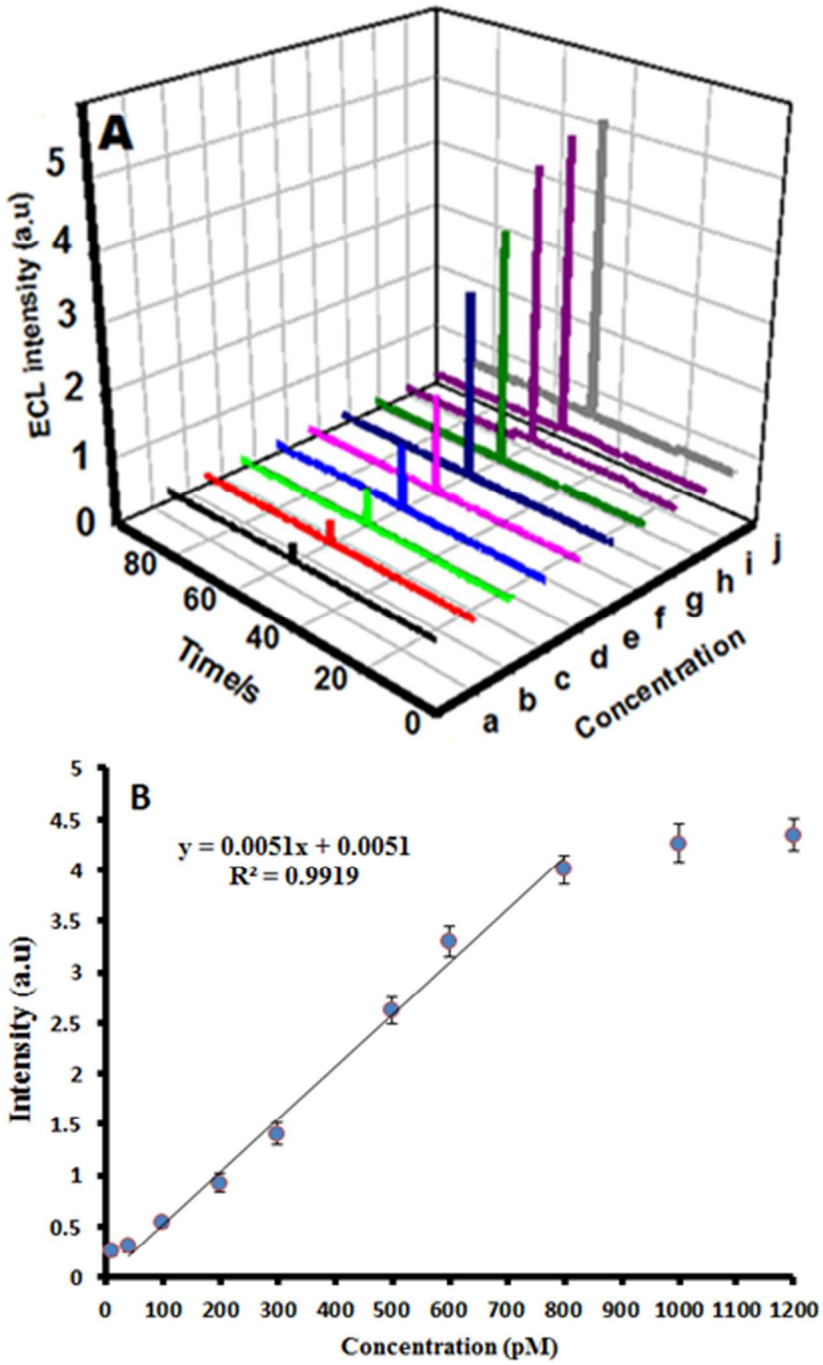
A
ECL intensity (a.u)
0
1
2
3
4
5
Time/s
0
20
40
60
80
Concentration
a
b
c
d
e
f
g
h
i
j
B
y = 0.0051x + 0.0051
R² = 0.9919
Intensity (a.u)
0
0.5
1
1.5
2
2.5
3
3.5
4
4.5
5
0
100
200
300
400
500
600
700
800
900
1000
1100
1200
Concentration (pM)

Figure 2.

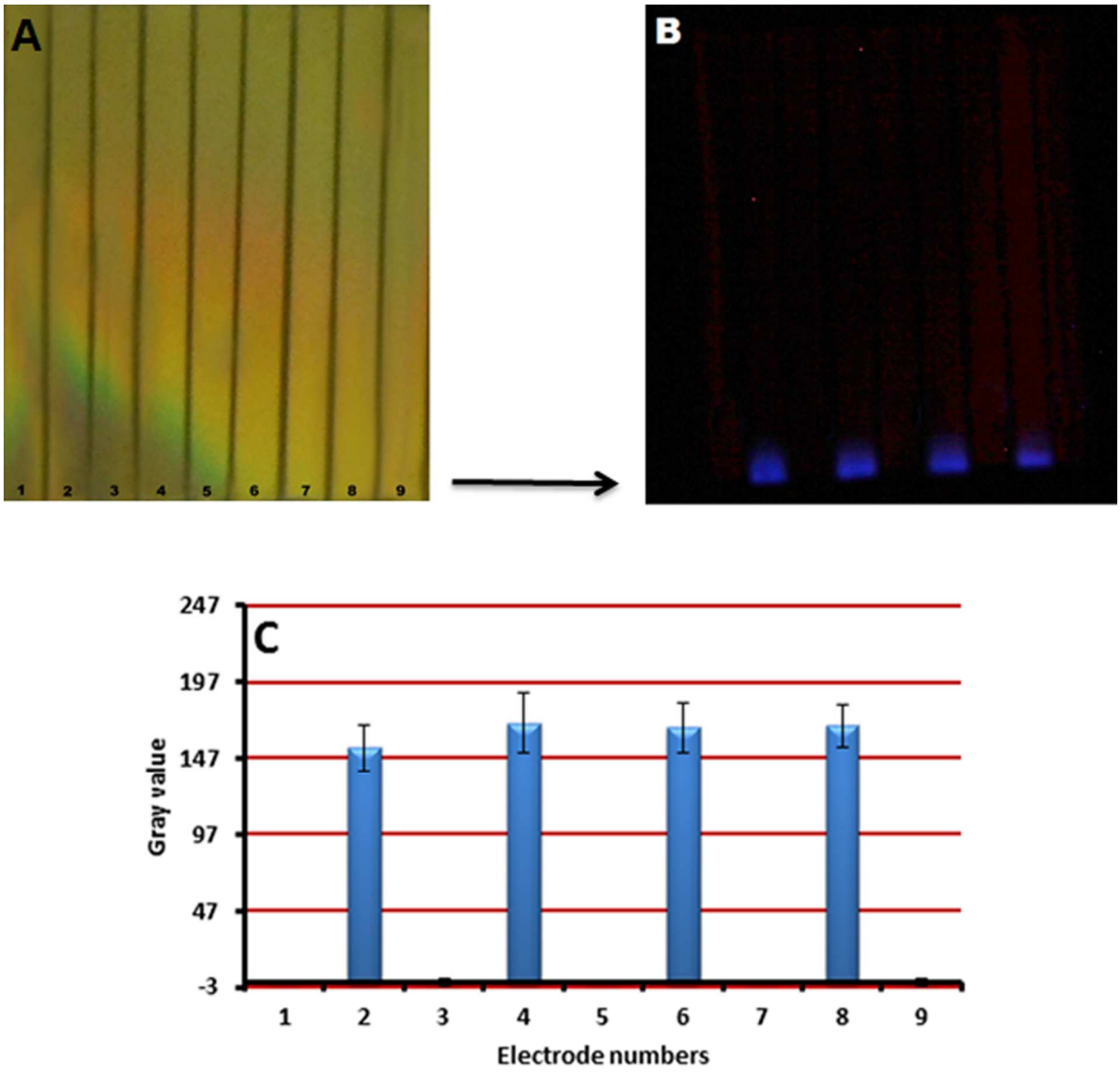
A
1 2 3 4 5 6 7 8 9
B
C
247
197
147
97
47
-3
Gray value
1 2 3 4 5 6 7 8 9
Electrode numbers

Figure 3.

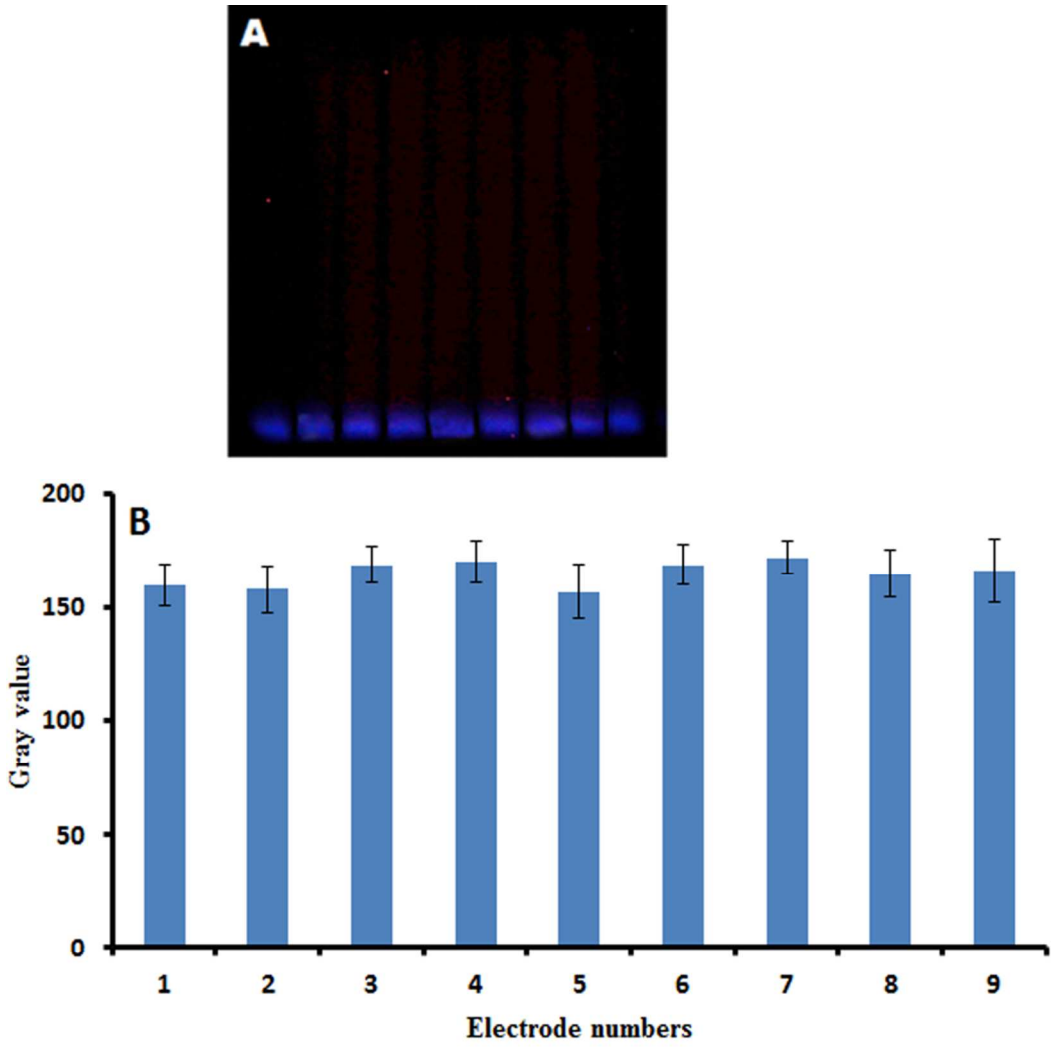

Figure 4.

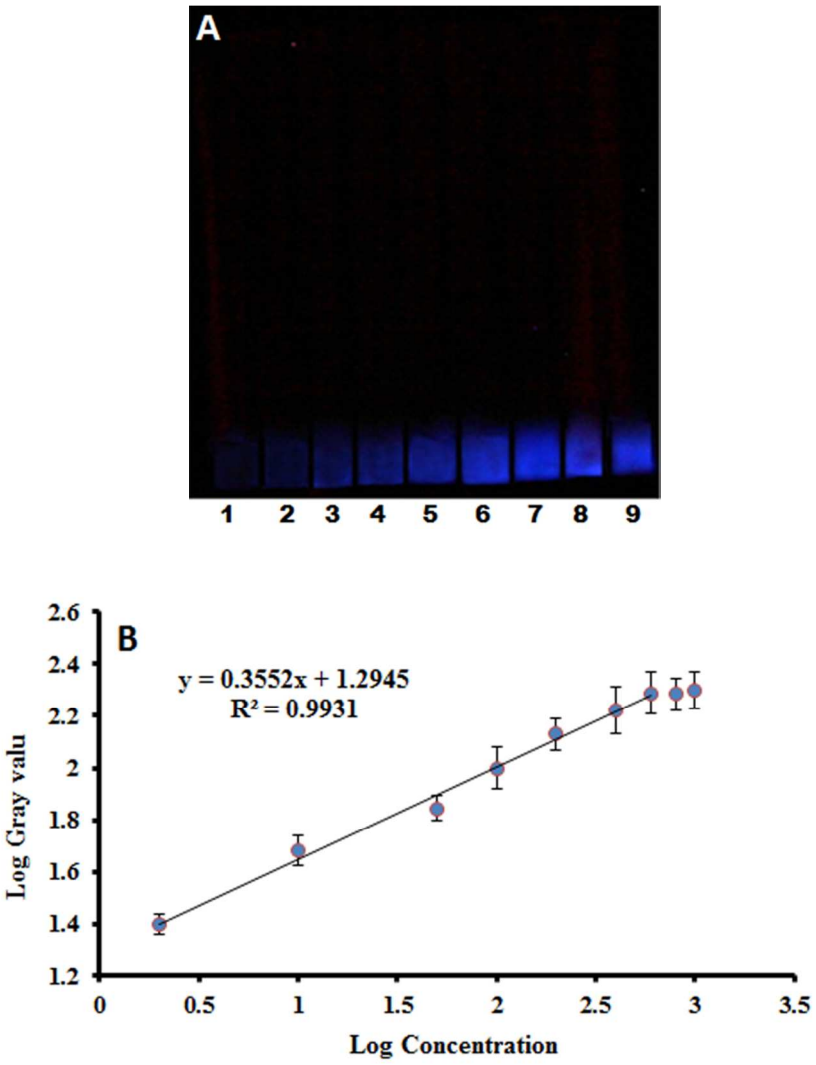
A
1 2 3 4 5 6 7 8 9
B
y = 0.3552x + 1.2945
R² = 0.9931
Log Gray valu
Log Concentration
2.6
2.4
2.2
2
1.8
1.6
1.4
1.2
0
0.5
1
1.5
2
2.5
3
3.5

Figure 5.

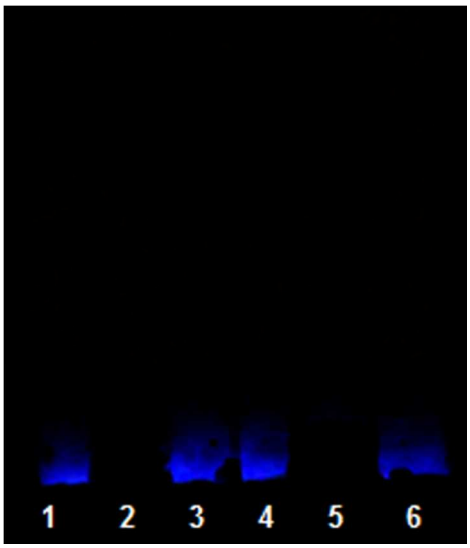

Figure 6.

“for TOC only”